Nanoscale

RSC Publishing

PAPER

View Article Online
View Journal | View Issue

Published on 28 March 2013. Downloaded by National Chiao Tung University on 28/04/2014 02:01:37.

Cite this: *Nanoscale*, 2013, **5**, 5086

Copper silicide/silicon nanowire heterostructures: *in situ* TEM observation of growth behaviors and electron transport properties†

Chung-Hua Chiu,[a] Chun-Wei Huang,[a] Jui-Yuan Chen,[a] Yu-Ting Huang,[a] Jung-Chih Hu,[b] Lien-Tai Chen,[b] Cheng-Lun Hsin[c] and Wen-Wei Wu*[a]

Received 23rd October 2012
Accepted 25th March 2013

DOI: 10.1039/c3nr33302g

www.rsc.org/nanoscale

Copper silicide has been studied in the applications of electronic devices and catalysts. In this study, Cu_3Si/Si nanowire heterostructures were fabricated through solid state reaction in an *in situ* transmission electron microscope (TEM). The dynamic diffusion of the copper atoms in the growth process and the formation mechanism are characterized. We found that two dimensional stacking faults (SF) may retard the growth of Cu_3Si. Due to the evidence of the block of edge-nucleation (heterogeneous) by the surface oxide, center-nucleation (homogeneous) is suggested to dominate the silicidation. Furthermore, the electrical transport properties of various silicon channel length with Cu_3Si/Si heterostructure interfaces and metallic Cu_3Si NWs have been investigated. The observations not only provided an alternative pathway to explore the formation mechanisms and interface properties of Cu_3Si/Si, but also suggested the potential application of Cu_3Si at nanoscale for future processing in nanotechnology.

Introduction

Nowadays, silicon-based technology is still the core of integrated circuits (IC) and follows the trace of Moore's law. Billions of transistors have been made on a single microprocessor chip. With the transition of device's dimension from microscale to 22 nanometers and further scaling down in the semiconductor industry, Si nanowire (NW) with metallic Schottky contact has been deemed as one of the alternative components for future nanoelectronics.[1–5] Excellent contact materials are crucial for modern electronics to achieve high performance and various functions. Metal silicides have been widely researched for their unique physical properties, ideal contact resistance, high quality of the interface with Si, and excellent compatibility with Si device processing.[6] With advances in nanoscale Si devices, nanostructures have unique physical properties and superior functions available because of the size effect. Low resistivity metal silicide NWs such as NiSi,[7–10] $NiSi_2$[11] and PtSi[12,13] have been demonstrated to be metallic contacts to Si nanostructures. Except for the electronic applications, silicide materials also have been widely explored in thermoelectric ($CrSi_2$)[14] and magnetic devices (Fe_3Si, CoSi)[15–17] with diverse structures, which have been demonstrated with various approaches including chemical vapor transport (CVT),[18,19] chemical vapor deposition (CVD),[17] solvothermal process,[20] and solid state reaction.[10,21] Among them, solid state reaction, which is the chemical reaction caused by interdiffusion of metal and Si atoms and subsequent phase transformation, has attracted great attention for the fabrication of nanowire heterostructure devices.[22,23] The phase transformation sequences of NWs have been found to deviate from that of bulk materials. Therefore, with research on silicide formation, it is more important to control the phase formation of the specific silicide nanostructures and to investigate their formation mechanisms and properties.

Since Dash (1956)[24] firstly used copper (Cu) to decorate dislocation in Si, Cu–Si interactions have been investigated widely for their microelectronic and catalytic applications.[25–29] Moreover, copper silicides would form at relatively lower processing temperatures than other silicide systems.[11] There are three equilibrium Cu–Si compounds, which are η''-Cu_3Si, $Cu_{15}Si_4$ and Cu_5Si at low temperatures, respectively. Among these, η''-Cu_3Si is the most commonly observed phase.[30] Cu_3Si comprises three polymorphs (η-, η'-, and η''-Cu_3Si phase) and can be transformed at different temperatures in the thin film system.[31,32] Recently, the growth morphology and mechanism of

[a]*Department of Materials Science and Engineering, National Chiao Tung University, No.1001, University Rd., East Dist., Hsinchu City 300, Taiwan. E-mail: wwwu@mail.nctu.edu.tw; Fax: +886-3-5724727; Tel: +886-3-5712121-55395*

[b]*Nanotechnology Research Center, Industrial Technology Institute (ITRI), Chutung, Hsinchu, Taiwan 31040, R.O.C*

[c]*Department of Electrical and Engineering, National Central University, Tao Yuan 320, Taiwan*

† Electronic supplementary information (ESI) available: Four ESI to demonstrate the fabrication procedures of *in situ* TEM samples, the temperature effect on copper silicide growth, different zone axis of η-Cu_3Si structure and derivation of activation energy. Three *in situ* TEM videos as ESI online material to present dynamic observation of the formation of η-Cu_3Si/Si/η-Cu_3Si nano-heterostructures. See DOI: 10.1039/c3nr33302g

 This journal is © The Royal Society of Chemistry 2013

Cu_3Si nanostructures in silicon have been reported.[33,34] However, the formation of Cu silicide nanostructures through solid state reaction and the investigation of the nanoscale kinetics are still unclear.

In this paper, the formation mechanism of Cu silicide NWs through solid state reaction has been investigated in the *in situ* TEM. The nanowire heterostructure at the interface was clearly evidenced to study the kinetics. Since the Cu silicides may serve as contacts and interconnects with Si channels in the nanoscale field effect transistor, the electron transport properties of the as-fabricated devices were also investigated.[35] This study could provide a potential approach for the formation of Cu silicides and the applications of the Cu_3Si/Si heterostructure as the metallic Schottky contact in future nano-transistors.

Experimental

Single crystalline silicon NWs with a high aspect ratio were grown on a Si wafer in the horizontal three zone furnace by vapor transport and condensation process *via* the vapor–liquid–solid (VLS) mechanism.[36,37] Au thin film was coated on the substrate as catalyst. During the growth process, (100) Si substrates were placed downstream at a temperature of 975 °C and Si powder was placed in an alumina boat at the upstream as precursor at a temperature of 1090 °C, respectively. Ar and H_2 were flown as carrier gases at the rate of 80 and 20 sccm, respectively. The pressure was adjusted to 20 Torr and the reaction time was held for 1 h. After the growth process in the furnace, Si NWs were detached from the wafer by ultrasonic vibration in ethanol solution and then dispersed on the SiO_2/Si_3N_4 membrane samples. Contact electrodes were prepared through e-beam lithography, copper deposition and lift-off processes (ESI, Fig. S-1†). Prior to Cu deposition, Si NW sample were dipped in buffered hydrofluoric acid for 30 seconds to etch surface native oxide in the contact region to prevent surface oxide from the barrier effect on the silicide formation at nanoscale.[11,12]

In situ observation of the solid state reaction through the contact electrodes and Si NWs was carried out in a Japan Electron Optics Laboratory 2100 FX (JEOL-2100 FX) TEM. The vacuum in the sample stage was about 3×10^{-8} Torr and the interfacial reaction process of the copper silicide/silicon NW heterostructures was performed at the temperature of 350 °C. The pressure during heating experiments was about 10^{-6} to 10^{-7} Torr, which resulted from the residual hydrocarbon and contaminant during the fabrication procedures of *in situ* TEM samples. The video recorder has a time resolution of 1/30 s and fast Fourier transform (FFT) technique was used to filter the noise of the high resolution images. The structural identification and morphology evolution of the pristine Si NWs and copper silicides were examined by a JEOL JSM-6500F field emission scanning electron microscope (FESEM) and JEOL 2100FX field emission scanning transmission electron microscope (STEM). Electrical transport measurement of the copper silicide/silicon NW heterostructures and copper silicide NWs were conducted by Agilent B1500A and Keithley 2400 system at room temperature in ambient conditions.

Results and discussion

Fig. 1(a) shows the SEM image of the as-grown products where high-density Si NWs with a high aspect ratio were grown on the substrate. Low magnification TEM image was shown in the inset of Fig. 1(a), indicating that the diameter of Si NW was about 80 nm with 2–5 nm native oxide and the Si–oxide interfaces was smooth (Fig. 1(b)). The high resolution TEM (HRTEM) image is utilized to characterize the crystal structure of the NWs (Fig. 1(b)). The inset is the corresponding FFT diffraction pattern, demonstrating that these NWs are characterized as single crystalline and ⟨111⟩ growth direction.

The schematic illustration of the device configuration is depicted in Fig. 2(a) and the inset was the configuration of the Si NW with Cu contact electrodes for the observation of the reaction of copper silicide/Si/copper silicide nano-heterostructures. Since Si NWs with various Si channel lengths were controlled and contained (highlighted regions of Fig. 2(b)), we could observe numerous examples simultaneously. Fig. 2(c) shows the TEM image of Si NW with Cu pads on both sides before heating. After annealing at 350 °C for several minutes, a high contrast interface between Cu silicide and Si began to emerge and approach from both edges of the Si NW near the Cu pads, suggesting the formation of Cu silicides (Fig. 2(d)). Therefore, we make the assumption that Cu atom would diffuse through the Cu–Si interface and dissolve into Si NW. Once the supersaturation point was reached, the subsequent nucleation and growth of Cu silicides would occur near the Cu pads. Deformation and detachment of NW from pads was found due to volume expansion when Si NW transformed into copper silicide NW that roughly increases the volume by 2.6 times. From the experimental results in Fig. 2(d), the axial length of the transformed η-Cu_3Si nanowire is about 1.1 times longer than that of the original Si nanowire, contributing to the deformation and detachment of nanowires. Furthermore, the silicide diameter increased by ∼1.45 times experimentally, which indicates that the 2.3 times volume expansion matches well with the theoretical value. The difference may be attributed to the surface oxide effect which could constrain the volume expansion and absorb part of the strain energy.[8] Based on the crystallography calculation and our FFT diffraction patterns, the epitaxial relation between η-Cu_3Si and Si was not observed; thus, a rough Si–η-Cu_3Si interface was found in Fig. 2(d).[33] Fig. 2(e) depicted the

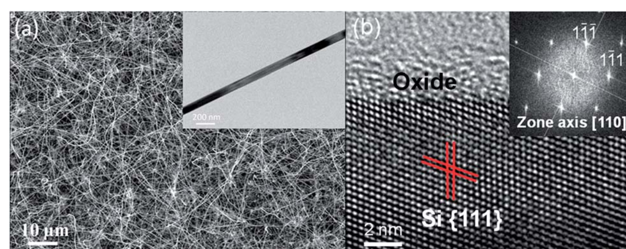

Fig. 1 (a) Low magnification SEM image of the as-grown Si NWs. The inset shows the corresponding TEM image. (b) HRTEM image of the Si NW. The inset is the FFT diffraction pattern, indicating the ⟨110⟩ zone axis of Si NW and ⟨111⟩ growth direction.

Published on 28 March 2013. Downloaded by National Chiao Tung University on 28/04/2014 02:01:37.

Published on 28 March 2013. Downloaded by National Chiao Tung University on 28/04/2014 02:01:37.

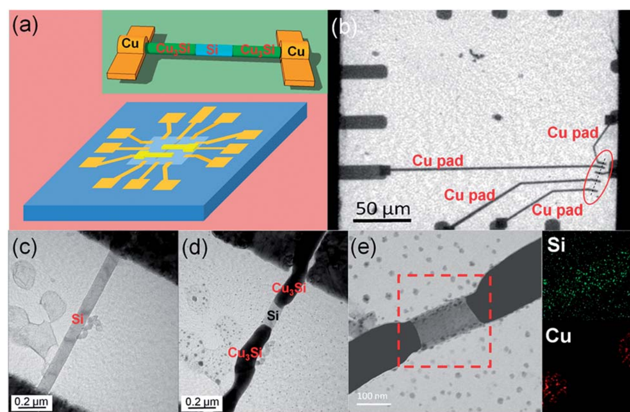

Fig. 2 (a) Schematic illustration of the device configuration with Si NW covered with Cu pads defined on the membrane. The inset shows the formation of copper silicide/Si/copper silicide nano-heterojunction. (b) The TEM image of the sample with a Si NW (indicated by dotted line) across several Cu pads with different electrode gaps (highlighted by red circle). (c) TEM image of a Si NW before the reaction. (d) TEM image of a Si NW after reaction showing the progression of the silicidation. (e) Bright-field STEM image of the interface between Cu_3Si and Si region. The inset shows the corresponding EDS mappings of Si and Cu.

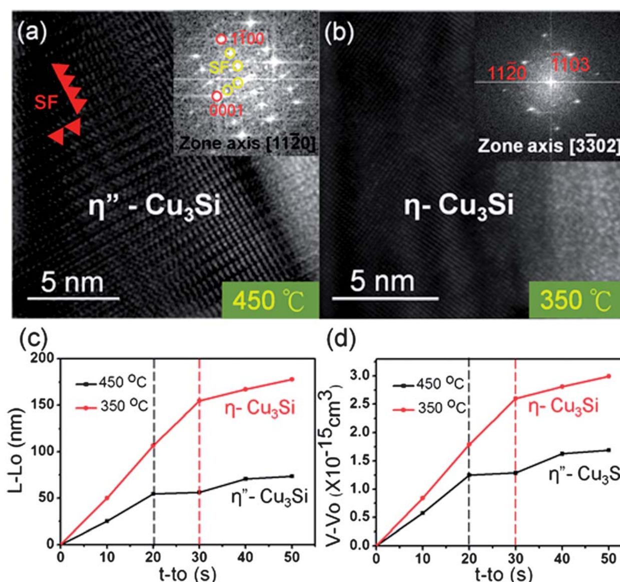

Fig. 3 HRTEM images of the polymorphs of (a) η″-Cu_3Si and (b) η-Cu_3Si at various reaction temperatures. The insets show the corresponding FFT diffraction patterns. Plot of (c) reaction length and (d) volume of Cu_3Si *versus* reaction time at 350 and 450 °C. The linear–parabolic transitions were indicated by black and red dashed lines, respectively.

bright-field STEM image of the interface between η-Cu_3Si and Si with enhanced Z-contrast. The insets illustrated the corresponding energy dispersion spectroscopy (EDS) mappings of Si and Cu (red-dashed square in Fig. 2(e)), which confirmed the emergence of Cu_3Si from the edge of Si NW and Cu pad instead of the center between two adjacent electrodes.

To investigate the effect of temperature on the growth of copper silicides, different temperatures were performed (ESI, Fig. S-2†). Meanwhile, the Cu_3Si phase with different polymorphs has been regarded as an interesting and promising research topic. HRTEM images of different polymorphs of Cu_3Si by various reaction temperatures of 450 and 350 °C were shown in Fig. 3(a) and (b), respectively. The insets are the corresponding FFT diffraction patterns of η″-Cu_3Si and η-Cu_3Si, respectively.[33] To further confirm the copper silicide structure grown at 350 °C, we have analyzed the η-Cu_3Si structure from higher symmetry zone axes (ESI, Fig. S-3†). From these zone axes and high-resolution TEM images, they still provided evidence that it is not η″-Cu_3Si phase although the same zone axis in Fig. 3(a) was not achieved. η-Cu_3Si is constructed with the hexagonal structure by lattice parameters of $a = 0.406$ nm and $c = 0.733$ nm, whereas the η″-Cu_3Si was a constituent with a periodic two-dimensional stacking fault (SF) of the η′ unit cell that has a superlattice structure of the η-Cu_3Si phase.[38] From the experimental results, the η″-Cu_3Si phase is found to have a high density of (1$\bar{1}$00) and (0001) plane stacking faults with about 1×10^7 cm^{-1} and 7×10^6 cm^{-1}, respectively. Furthermore, this information provides evidence that the phase transformation between three polymorphs of Cu_3Si under different temperatures is quite distinct from the previous study in the thin film system.[32] It suggested that the atomic interaction could be greatly deviated in one dimensional nanostructures. Additionally, the structural crystallinity variant may attribute to the change of activation energy and equilibrium phase sequence from the thin film system.[39] Fig. 3(c) is the plot of the growth length as the function of reaction time at various temperatures, illustrating two different growth rates in the solid state reaction of Cu and Si NWs. At the beginning of the reaction, roughly linear growth rates were presented. It means that the growth process was mainly controlled by an interface-limited reaction instead of a diffusion-limited reaction at the first step. However, owing to the difference of the diffusivity coefficient of Cu in Si and Cu_3Si, the linear growth rate may transform into parabolic growth behavior at the following step. Followed by the hypothesis we had proposed, the growth rate should increase with increasing temperature. However, it is confusing that the reaction rate at 450 °C is much slower than that at 350 °C (ESI, Video-1 and 2†). To elucidate the nano-sized effect by the variable diameters of the NWs, the plot of the copper silicide volume *versus* reaction time at various temperatures is shown in Fig. 3(d), exhibiting a significant decrease of the growth rate with the temperature at 450 °C.

To explain this phenomenon, the modified kinetic model deduced from Chen *et al.* was applied.[40] For a short growth time (t), the growth length (L) of Cu_3Si is given in the following form:

$$L = \frac{MCKt}{b\rho}$$

where M is the atomic weight of Cu_3Si, C is the Cu concentration per unit volume at the Cu–Cu_3Si interface, K is the reaction rate constant, ρ is density, and b is the number of Cu atoms in the molecular formula, respectively. Since all polymorphs of Cu_3Si have a similar molecular formula and crystal structure, M and b are identical. In addition, the density ρ of η″- and η-Cu_3Si phase can be considered the same.[38] Cu concentration per unit volume C is constant based on the assumption of steady state and

 This journal is © The Royal Society of Chemistry 2013

Published on 28 March 2013. Downloaded by National Chiao Tung University on 28/04/2014 02:01:37.

infinite Cu source. Specifically, if other parameters are constants in the reactions, the growth rate is proportional to the reaction rate constant K, which is the function of temperature. Consequently, the growth rate at a temperature of 450 °C should be faster than that of 350 °C, whereas it is quite different in reality. When the temperature is higher, the mobility of dislocation increases, resulting in the dissociation of a perfect dislocation into two partials. The dislocation inside the NW may attribute to the incoherent Cu_3Si–Si interface. We attributed the striking kinetics results to the additional energy necessary to form two dimensional SF after the formation of a new Cu_3Si nucleation layer. Therefore, the reaction rate constant at 450 °C is considered smaller than that at 350 °C. The additional energy may be attributed to the repulsive force between two partial dislocations and surface free energy (surface tension) of SF, which contributes to the higher activation energy. Furthermore, the spacing of SF fringes is a competitive balance between the repulsive force of two partial dislocations and the attractive force due to the surface tension of the stacking fault. It resulted in the growth rate at the temperature of 450 °C declining more compared with that at 350 °C. In a one dimensional structure, the size effect could be the driving force for the η''-Cu_3Si phase to form in the first place at relatively high temperature, and the phase transformation between the three polymorphs of Cu_3Si. This is attributed to the atomic motion being different to the one dimensional nanostructure from the previous study in the thin film system.[32] Furthermore, the phase transformation sequence in one dimensional metal silicide nanostructures have been found to deviate from that of bulk and thin film systems.[11,42] On the other hand, the dissociation of a perfect dislocation into two partials may be another driving force, resulting from a lower gliding energy of partial dislocations. The yield of finding the SF structure at 450 °C is about 60–70%, whereas it is rare to find SF at 350 °C. In addition, the effect of the stacking faults on the activation energy would also be observed on the diffusion process in which the linear–parabolic transition occurred significantly and was indicated by the black dashed line in Fig. 3(c) and (d). More detailed experimental studies and discussion on this system are necessary to make a thorough conclusion.

The growth kinetics of Cu silicide in Si NW was investigated through dynamic observation by *in situ* HRTEM (ESI, Video-3†). Fig. 4(a) is an image during the growth of η-Cu_3Si and highlighted with a red-dash lines at the boundary of Si, oxide and η-Cu_3Si after being annealed at 350 °C. This observation was similar to the previous study.[41] It is assumed that the surface energy of the oxide–silicide interface is higher than that of the oxide–silicon interface because of the surface native oxide. Therefore, when Cu silicide frontier approaches the edge of the Si NW, it will be hindered before the edge transformed to the oxide–silicide interface resulting from high energy barrier. Fig. 4(b) is the schematic diagram of the curved interface at the triple point of Si, surface oxide and η-Cu_3Si. Meanwhile, this result also suggested that the nucleation mechanism was possibly center-nucleation (homogeneous) rather than edge-nucleation (heterogeneous) since the

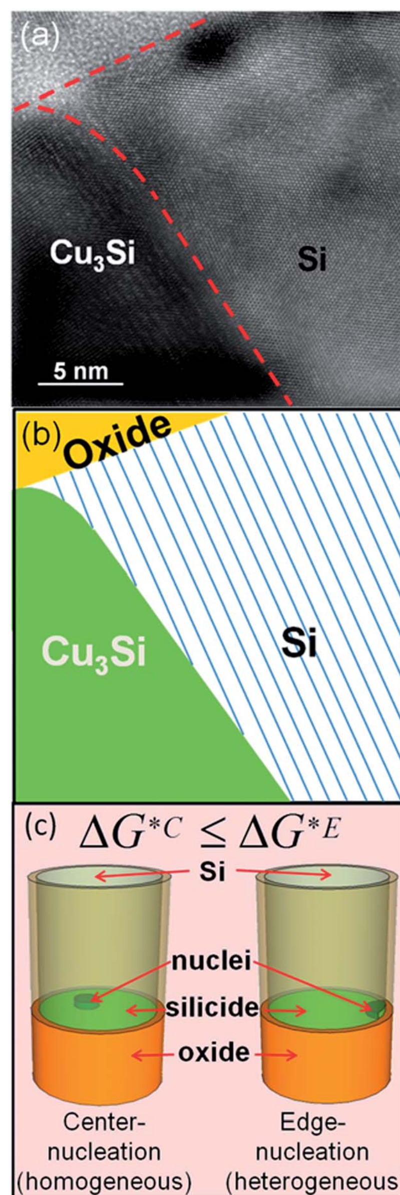

Fig. 4 (a) HRTEM image of η-Cu_3Si after 350 °C annealing shows a curved interface near the oxide edge. (b) Schematic diagram of the curved interface at the triple point. (c) The cross-sectional view of the schematic illustration of the center-nucleation (homogeneous) site and the edge-nucleation (heterogeneous) site.

variation in the net change of free energy is described in the following equations:

$$\Delta G^{C} = (V_{disc}\Delta g_{v} + A^{C}_{silicide/Si}\gamma^{C}_{silicide/Si})$$

$$\Delta G^{E} = (V_{disc}\Delta g_{v} + A^{E}_{silicide/Si}\gamma^{E}_{silicide/Si} + A^{E}_{silicide/oxide}\gamma^{E}_{silicide/oxide} - A^{E}_{Si/oxide}\gamma^{E}_{Si/oxide})$$

where ΔG^{C} and ΔG^{E} are the net change in the free energy of the center and edge-nucleations, V_{disc} is the critical volume of nuclei when the nucleation occurred, Δg_v is the change in free energy of formation of the silicide per unit volume, A is the additional interface area, and γ is the interfacial energy per unit area, respectively. The upper and lower cases in these notations

denote the different nucleation site and interface, respectively. The nucleation type we discussed at η-Cu_3Si–Si interface was focused on a newly/initially nucleated η-Cu_3Si atomic layer. Therefore, the diameter of the η-Cu_3Si nanowire close to the η-Cu_3Si–Si interface will be similar to that of the original Si nanowire as shown in Fig. 2(d) and (e). From the experimental results as shown in Fig. 4(a) and Video-3,† every new η-Cu_3Si atomic layer always started from the center of the Si NW. It revealed that the homogeneous nucleation dominates the η-Cu_3Si growth. Furthermore, the homogeneous nucleation of silicide growth has been demonstrated in our previous studies.[41,42] Therefore, we consider that activation energy inequality, $\Delta G^{*C} \leq \Delta G^{*E}$, will be satisfied as illustrated in Fig. 4(c) where the edge-nucleation (heterogeneous) of Cu_3Si is considered to be suppressed (further discussion is shown in Fig. S-4†).

Based on such Cu_3Si/Si/Cu_3Si nanoheterostructures, the electrical transport properties of several Si channel lengths were also investigated. Fig. 5(a) is the low magnitude TEM image of the device with different electrode gaps, and η-Cu_3Si/Si/η-Cu_3Si with variable channel lengths controlled by solid-state reaction at 350 °C, which are 235 nm, 1.2 μm and 2.3 μm, respectively (Fig. 5(b)–(d)). The current output of each channel lengths as shown in Fig. 6(a), indicating that the current increased as the channel length decreased. Contact resistance determined by linear extrapolation of the total resistance *versus* various channel lengths with the value 2.827×10^7 Ω was indicated in Fig. 6(b). The intrinsic resistivity of Si NW was calculated by the reciprocal slope of *I*–*V* curve at nearly $V = 0$ (Fig. 6(a)). Under the exclusion of contact resistances, the intrinsic resistivity of Si NW was about 18.15 Ω-cm determined by the law of resistance,

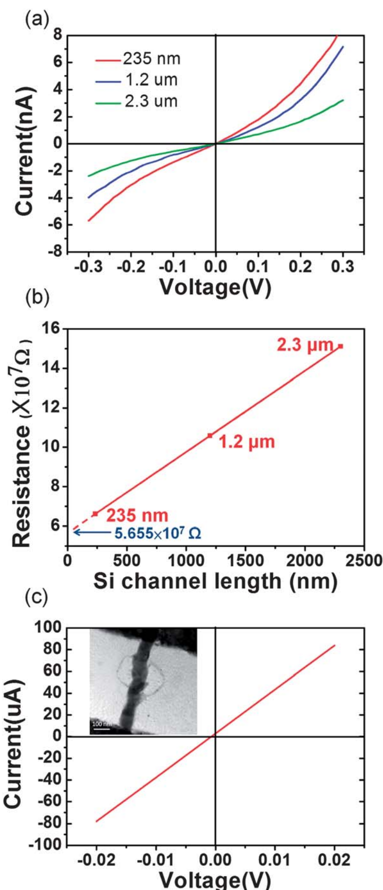

Fig. 6 (a) The electrical transport measurements of η-Cu_3Si/Si/η-Cu_3Si devices with different channel length from solid-state reactions. (b) The total resistance *versus* various channel lengths that indicate the contact resistance of 2.827×10^7 Ω. (c) The electrical transport measurement of metallic η-Cu_3Si NW with 206 μΩ cm resistivity. The inset is the corresponding TEM image of η-Cu_3Si NW after fully silicidation.

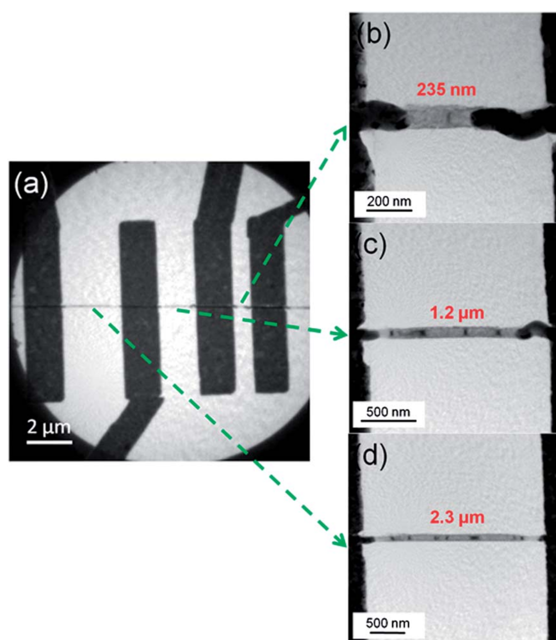

Fig. 5 (a) Low magnitude TEM image of η-Cu_3Si/Si/η-Cu_3Si nano-heterostructure device. (b)–(d) Variable channel lengths formed by solid-state reaction at 350 °C with the length of 235 nm, 1.2 μm and 2.3 μm, respectively.

which compared favorably with the previously reported values in bulk materials. It may be attributed to the single crystal Si NW grown in this study. *I*–*V* characteristics of several metallic η-Cu_3Si/Si/η-Cu_3Si nanowire heterostructures depicted the Schottky-diode-like (SDL) behavior. The effective barrier height Φ_B was calculated through the thermionic emission theory which can be expressed as follows:

$$J_S = A^* T^2 \exp\left(\frac{-e\Phi_B}{kT}\right) (\text{A cm}^{-2})$$

where J_S is the saturation current density, A^* is the Richardson constant, T is the temperature in Kelvin, e is the electron charge, and k is Boltzmann's constant, respectively.[43]

Because of surface states and the intrinsic p-type characteristics of Si NWs attributed to the hole accumulation, the Richardson constant with a value of 80 A cm^{-2} K^{-2} for p-Si was assumed. Based on the equation and values, Φ_B of η-Cu_3Si–Si interface was extracted with a value of 0.41 eV which may be the origin of the SDL behaviors. The electrical measurement of an intact η-Cu_3Si NW was also investigated after full silicidation, as shown in Fig. 6(c). The *IV* curve indicated that the measured resistivity was about 206 μΩ cm by using two-terminal

Published on 28 March 2013. Downloaded by National Chiao Tung University on 28/04/2014 02:01:37.

This journal is © The Royal Society of Chemistry 2013

View Article Online

Published on 28 March 2013. Downloaded by National Chiao Tung University on 28/04/2014 02:01:37.

measurement, which may include the contact resistance between probes and NWs.[7,13] This value compared favorably to the previous study (272 μΩ cm and 21μΩ cm for two and four-terminal measurements).[44] Therefore, the intrinsic resistivity of η-Cu_3Si NW should be favorably compatible to other silicide systems in one-dimensional structures. Significantly, single crystal Cu_3Si NWs with low resistivity may have potential application as an electronic contact material in future nano-transistors.

Conclusions

Single-crystalline Si NWs were synthesized through a thermal evaporation and condensation method *via* VLS mechanism. The polymorphs of Cu_3Si phases and Cu_3Si/Si nano-heterostructures were formed through a solid state reaction at different temperatures. In addition, the plot of the growth rate suggests that Cu_3Si has a linear–parabolic transition behavior. Meanwhile, it is assumed that the formation of two dimensional stacking faults within the Cu_3Si NW may retard the growth rate owing to higher activation energy for η″-Cu_3Si growth. During the growth, the nucleation is thought to be center-nucleation (homogeneous) rather than edge-nucleation (heterogeneous) due to the presence of the surface native oxide and the oxide/silicide interfacial energy. Furthermore, the correlation between the current output and the remaining Si channel has been investigated and intrinsic resistivity of Si NW was calculated to be 18.15 Ω cm with the exclusion of contact resistance. According to the thermionic emission theory, Φ_B of Cu_3Si–Si interface is extracted to be 0.41 eV, which may contribute to the Schottky contact like behaviors. Additionally, electrical measurement of η-Cu_3Si NW shows a resistivity of around 206 μΩ cm by two-terminal measurement. The true value may be lower than the counterpart of the thin film if the extrinsic series resistances are excluded. This study demonstrates the synthesis of Cu_3Si NW through solid state reaction and could contribute to the electronic applications. The nanowire heterostructures may have potential applications in metallic Schottky source–drain and the fundamentals of nanowire heterostructure formation are of great importance for future device fabrication.

Acknowledgements

W.W.W. and C.L.H. acknowledge the support by National Science Council through grants 100-2628-E-009-023-MY3, and 101-2218-E-008-014-MY2.

Notes and references

1 J. Hahm and C. M. Lieber, *Nano Lett.*, 2004, **4**, 51–54.
2 Y. N. Xia, P. D. Yang, Y. G. Sun, Y. Y. Wu, B. Mayers, B. Gates, Y. D. Yin, F. Kim and Y. Q. Yan, *Adv. Mater.*, 2003, **15**, 353–389.
3 Y. Cui and C. M. Lieber, *Science*, 2001, **291**, 851–853.
4 M. N. Masood, S. Chen, E. T. Carlen and A. van den Berg, *ACS Appl. Mater. Interfaces*, 2010, **2**, 3422–3428.
5 F. Patolsky, G. F. Zheng, O. Hayden, M. Lakadamyali, X. W. Zhuang and C. M. Lieber, *Proc. Natl. Acad. Sci. U. S. A.*, 2004, **101**, 14017–14022.
6 H. Jiang, C. M. Osburn, P. Smith, Z. G. Xiao, D. Griffis, G. Mcguire and G. A. Rozgonyi, *J. Electrochem. Soc.*, 1992, **139**, 196–206.
7 Y. Wu, J. Xiang, C. Yang, W. Lu and C. M. Lieber, *Nature*, 2004, **430**, 61–65.
8 W. W. Wu, K. C. Lu, K. N. Chen, P. H. Yeh, C. W. Wang, Y. C. Lin and Y. Huang, *Appl. Phys. Lett.*, 2010, **97**, 203110.
9 W. W. Wu, K. C. Lu, C. W. Wang, H. Y. Hsieh, S. Y. Chen, Y. C. Chou, S. Y. Yu, L. J. Chen and K. N. Tu, *Nano Lett.*, 2010, **10**, 3984–3989.
10 K. C. Lu, K. N. Tu, W. W. Wu, L. J. Chen, B. Y. Yoo and N. V. Myung, *Appl. Phys. Lett.*, 2007, **90**, 253111.
11 Y. C. Lin, Y. Chen, D. Xu and Y. Huang, *Nano Lett.*, 2010, **10**, 4721–4726.
12 K. C. Lu, W. W. Wu, H. Ouyang, Y. C. Lin, Y. Huang, C. W. Wang, Z. W. Wu, C. W. Huang, L. J. Chen and K. N. Tu, *Nano Lett.*, 2011, **11**, 2753–2758.
13 Y. C. Lin, K. C. Lu, W. W. Wu, J. W. Bai, L. J. Chen, K. N. Tu and Y. Huang, *Nano Lett.*, 2008, **8**, 913–918.
14 F. Zhou, J. Szczech, M. T. Pettes, A. L. Moore, S. Jin and L. Shi, *Nano Lett.*, 2007, **7**, 1649–1654.
15 J. Herfort, H. P. Schonherr and K. H. Ploog, *Appl. Phys. Lett.*, 2003, **83**, 3912–3914.
16 K. Seo, K. S. K. Varadwaj, P. Mohanty, S. Lee, Y. Jo, M. H. Jung, J. Kim and B. Kim, *Nano Lett.*, 2007, **7**, 1240–1245.
17 Y. H. Liang, S. Y. Yu, C. L. Hsin, C. W. Huang and W. W. Wu, *J. Appl. Phys.*, 2011, **110**, 074302.
18 J. R. Szczech, A. L. Schmitt, M. J. Bierman and S. Jin, *Chem. Mater.*, 2007, **19**, 3238–3243.
19 Y. P. Song, A. L. Schmitt and S. Jin, *Nano Lett.*, 2007, **7**, 965–969.
20 J. H. Ma, Y. L. Gu, L. Shi, L. Y. Chen, Z. H. Yang and Y. T. Qian, *J. Alloys Compd.*, 2004, **376**, 176–179.
21 K. C. Lu, W. W. Wu, H. W. Wu, C. M. Tanner, J. P. Chang, L. J. Chen and K. N. Tu, *Nano Lett.*, 2007, **7**, 2389–2394.
22 Y. C. Lin, Y. Chen and Y. Huang, *Nanoscale*, 2012, **4**, 1412–1421.
23 C. L. Hsin, W. F. Lee, C. T. Huang, C. W. Huang, W. W. Wu and L. J. Chen, *Nano Lett.*, 2011, **11**, 4348–4351.
24 W. C. Dash, *J. Appl. Phys.*, 1956, **27**, 1193–1195.
25 M. O. Aboelfotoh and L. Krusinelbaum, *J. Appl. Phys.*, 1991, **70**, 3382–3384.
26 F. Bernard, H. Souha and E. Gaffet, *Mater. Sci. Eng., A*, 2000, **284**, 301–306.
27 N. Selamoglu, J. A. Mucha, D. L. Flamm and D. E. Ibbotson, *J. Appl. Phys.*, 1988, **64**, 1494–1498.
28 A. Cros, M. O. Aboelfotoh and K. N. Tu, *J. Appl. Phys.*, 1990, **67**, 3328–3336.
29 C. Y. Wen, M. C. Reuter, J. Tersoff, E. A. Stach and F. M. Ross, *Nano Lett.*, 2010, **10**, 514–519.
30 R. R. Chromik, W. K. Neils and E. J. Cotts, *J. Appl. Phys.*, 1999, **86**, 4273–4281.

This journal is © The Royal Society of Chemistry 2013

Published on 28 March 2013. Downloaded by National Chiao Tung University on 28/04/2014 02:01:37.

31 G. Weber, B. Gillot and P. Barret, *Phys. Status Solidi A*, 1983, **75**, 567–576.
32 J. K. Solberg, *Acta Crystallogr., Sect. A: Cryst. Phys., Diffr., Theor. Gen. Crystallogr.*, 1978, **34**, 684–698.
33 S. Li, H. Cai, C. L. Gan, J. Guo, Z. Dong and J. Ma, *Cryst. Growth Des.*, 2010, **10**, 2983–2989.
34 Z. Zhang, L. M. Wong, H. G. Ong, X. J. Wang, J. L. Wang, S. J. Wang, H. Y. Chen and T. Wu, *Nano Lett.*, 2008, **8**, 3205–3210.
35 E. Lind, A. I. Persson, L. Samuelson and L. E. Wernersson, *Nano Lett.*, 2006, **6**, 1842–1846.
36 R. S. Wagner and W. C. Ellis, *Appl. Phys. Lett.*, 1964, **4**, 89.
37 J. B. Hannon, S. Kodambaka, F. M. Ross and R. M. Tromp, *Nature*, 2006, **440**, 69–71.
38 C. Y. Wen and F. Spaepen, *Philos. Mag.*, 2007, **87**, 5581–5599.
39 V. C. Holmberg, M. G. Panthani and B. A. Korgel, *Science*, 2009, **326**, 405–407.
40 Y. Chen, Y. C. Lin, C. W. Huang, C. W. Wang, L. J. Chen, W. W. Wu and Y. Huang, *Nano Lett.*, 2012, **12**, 3115–3120.
41 Y. C. Chou, W. W. Wu, L. J. Chen and K. N. Tu, *Nano Lett.*, 2009, **9**, 2337–2342.
42 Y. C. Chou, W. W. Wu, C. Y. Lee, C. Y. Liu, L. J. Chen and K. N. Tu, *J. Phys. Chem. C*, 2011, **115**, 397–401.
43 W. Mönch, *Electronic Properties of Semiconductor Interfaces*, Springer, Berlin, 2004.
44 S. J. Jung, T. Lutz, A. P. Bell, E. K. McCarthy and J. J. Boland, *Cryst. Growth Des.*, 2012, **12**, 3076–3081.

 This journal is © The Royal Society of Chemistry 2013